We are IntechOpen, the world's leading publisher of Open Access books Built by scientists, for scientists

4,800
Open access books available

122,000
International authors and editors

135M
Downloads

Our authors are among the

154
Countries delivered to

TOP 1%
most cited scientists

12.2%
Contributors from top 500 universities

CLARIVATE ANALYTICS BOOK CITATION INDEX INDEXED

WEB OF SCIENCE™

Selection of our books indexed in the Book Citation Index in Web of Science™ Core Collection (BKCI)

Interested in publishing with us?
Contact book.department@intechopen.com

Numbers displayed above are based on latest data collected.
For more information visit www.intechopen.com

Chapter

Development and Control of Generator-Converter Topology for Direct-Drive Wind Turbines

Akanksha Singh

Abstract

In this chapter, a new topology for Direct-Drive Wind Turbines (DDWTs) with a low-voltage generator design is presented in order to eliminate the required dc-bus capacitors or dc-link inductors. In the presented topology, the grid-side converter is replaced by a boost Current Source Inverter (CSI) therefore removing the need for the dc-bus electrolytic capacitors which results in increasing the system lifetime. In the developed topology, the synchronous inductance of the generator is utilized. This facilitates the elimination of the intrinsically required dc-link inductor in the CSI which further contributes to a reduction in the overall system weight and size. The boost CSI is capable of converting a low dc voltage to a higher line-to-line voltage. This results in the implementation of a low-voltage generator for DDWTs. The feasibility of the presented low-voltage generator is investigated through Finite Element (FE) computations. In this chapter, a modified 1.5 MW low-voltage generator for the proposed topology is compared with an existing 1.5 MW Permanent Magnet (PM) synchronous generator for DDWTs. The feasibility of the presented topology of generator-converter for DDWTs is verified through simulations and laboratory tests. Furthermore, the controls developed for the developed wind turbine topology is also presented in this chapter.

Keywords: boost CSI, direct-drive wind turbine, finite element analysis, permanent magnet synchronous generator, wind turbine topologies

1. Introduction

Wind power is one of the fastest growing energies and the global capacity has increased to 433 GW by the end of 2015 [1, 2]. The two most commonly used topologies for wind turbines are based on the Doubly Fed Induction Generator (DFIG) or Permanent Magnet Synchronous Generator (PMSG) [3]. In the DFIG configuration, the stator of the generator is directly connected to the grid while the rotor does not require to rotate at the fixed synchronous speed. The rotor is connected to the turbine shaft through a gearbox. In the PMSG-based wind turbines, the speed of the rotating magnetic field and the rotor is the same and therefore, it is connected to the grid through power converters. The PMSG-based wind turbines require a power electronics interface to be connected to the grid which provides the flexibility of using these turbines with or without gearbox between the turbine shaft and the generator shaft [3]. It has been shown that the gearboxes cause more

downtime than any other component in a wind turbine [3–5]. It is worth noting that the gearboxes are responsible for 10% of the wind turbine failures which result in about 20% of the total wind turbine downtime [4–6]. Recent investigations reveal that gearboxes in wind turbines, which were supposed to last 20 years, might fail in 7–10 years [7, 8]. The Direct-Drive Wind Turbines (DDWTs) do not have a gearbox between the turbine rotor and the generator shaft. There is a definite trend toward DDWTs as is predicted in the research papers and trade articles but there are some major concerns that must be overcome in order to achieve higher market penetration [1, 9]. The power electronics interface in a DDWT is rated for full power transfer and it consists of an active rectifier and a grid-side converter, connected through a capacitor bank forming the dc-bus. The power electronics interface is one of the most vulnerable components in wind turbines [4, 5, 7]. A significant percentage of these failures have been attributed to the dc-bus electrolytic capacitors [10, 11]. Many methods which try to determine the remaining lifespan of electrolytic capacitors exist and are utilized for scheduled maintenance planning [5]. These methods do not serve to extend the life of the capacitors and contribute to an increase in the system downtime [7]. The other major concern which prevents the proliferation of DDWTs is the large size of PMSGs [12, 13]. The large size of the generator is a result of the generator shaft rotating at the same speed as the turbine rotor shaft. The low angular speed in PMSGs increases the required pole surface and the number of poles, which results in a high cost and volume of the generator.

In the most commonly used DDWT configuration the power electronics interface comprises of back-to-back Voltage Source Converters (VSCs) connected through electrolytic capacitors [14]. In this paper, the grid-side VSC is replaced by the boost Current Source Inverter (CSI). The proposed boost CSI topology of the converter results in the elimination of the dc-bus electrolytic capacitors, which are one of the frequently failing components in the existing topologies of direct-drive wind turbines without any supplementary component at the dc-bus [10, 11, 15]. The boost CSI converts the low dc voltage of the generator rectifier to the higher voltage level which facilitates the implementation of low voltage PMSG with lower weight and volume [16]. In addition to the introduction, this chapter has five more sections. In Section 2, the existing wind turbine topologies are reviewed, and the topology of the developed system is introduced. Section 3 presents the feasibility of a 1.5 MW low-voltage PMSG for the presented system. This section also presents a comparison between the generator for the developed system and an existing 1.5 MW PMSG for a DDWT using Finite Element (FE) computations. The controls developed for the new DDWT topology are presented in Section 4. The simulation results demonstrating the feasibility of the developed system are presented in Section 5. A laboratory scale setup is used to experimentally confirm the feasibility of the proposed topology in Section 6. Section 7 presents the conclusions of the chapter.

2. Wind turbine topologies

In this section, several wind turbine topologies are reviewed prior to introducing the inductorless current source generator-converter topology.

2.1 Indirect drive wind turbine topologies

In the majority of wind turbine topologies, the windmill rotor shaft is connected to the generator through a gearbox [14, 17]. The indirect drive wind turbines can be assembled using various types of generators and converters. Most commonly

used indirect wind turbine utilizes the DFIG configuration of the drivetrain. In this configuration, the rotor is connected to the grid through a back-to-back converter while the stator windings are directly connected to the grid and. This back-to-back converter includes of two bidirectional converters connected at the dc-bus, which formed by a capacitor bank. In this configuration, the major part of the power injected into the grid is through the stator of the generator and the back-to-back converters transfer only a fraction of the power produced by the wind turbine into the grid. The PMSG with the same back-to-back converter topology is another common indirect drive wind turbine topology. Unlike in the DFIG configuration, the converter is rated for the full power.

2.2 Direct drive wind turbine (DDWT) topologies

The DDWT is a relatively new topology and has the turbine rotor shaft directly connected to the generator shaft without any gearbox. **Figure 1** shows commonly used topologies for DDWTs using the PMSG. **Figure 1(a)** displays the power electronics interface which consists of a diode bridge rectifier, dc-dc boost converter, and grid-tied VSC [17, 18]. **Figure 1(b)** shows another DDWT topology with power electronics interface consisting of grid-tied back-to-back Current Source Converters (CSCs) connected through a dc-link inductor [19, 20]. **Figure 1(c)** demonstrates the most frequently used configuration of DDWTs, comprising of a PMSG connected

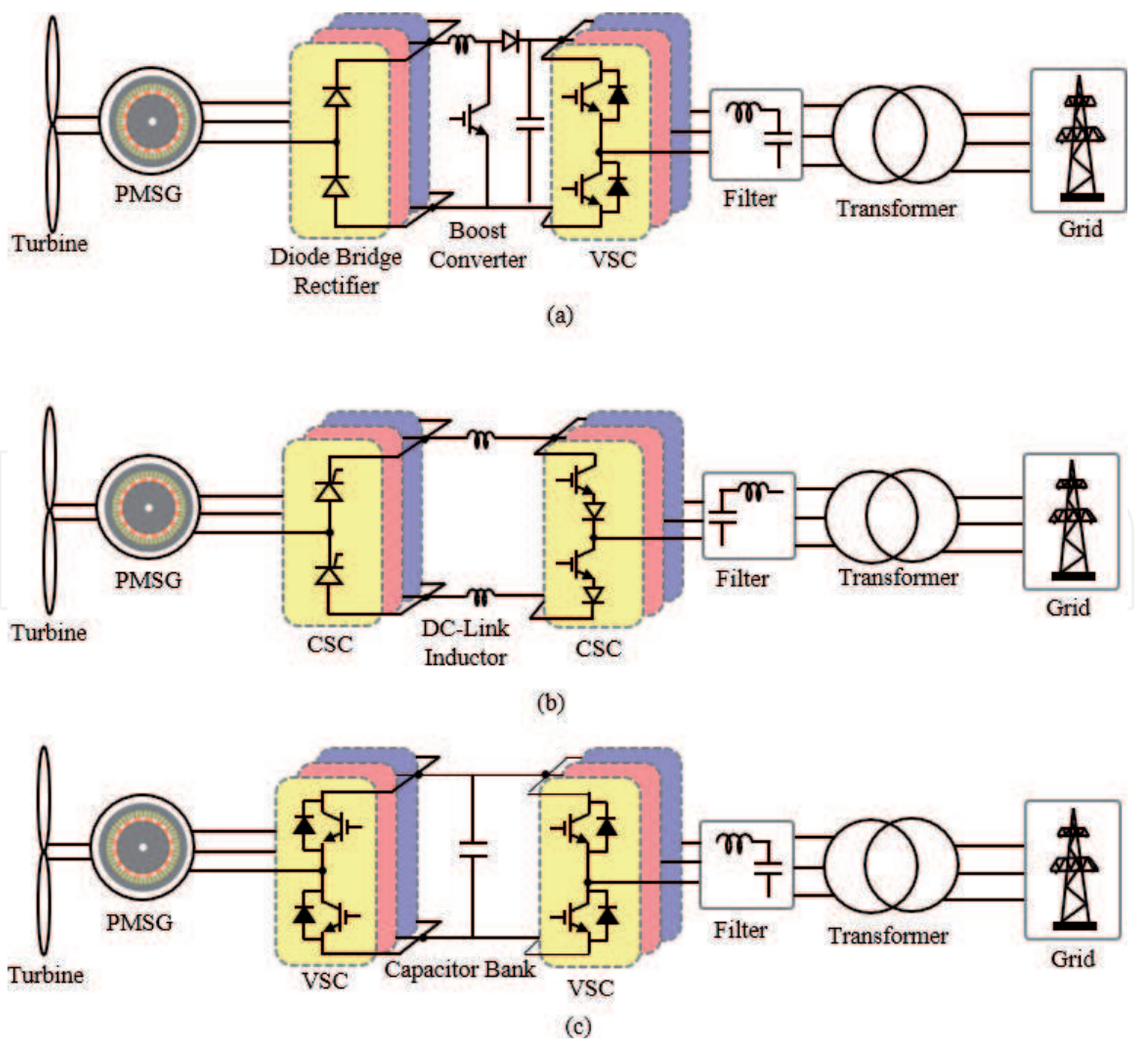

Figure 1.
Common DDWT topologies with (a) PMSG connected to diode-bridge, boost converter and VSI, (b) PMSG connected to back-to-back CSCs, and (c) PMSG connected to back-to-back VSCs.

to the grid through two VSCs [17, 21, 22]. The dc-bus between the VSCs is formed using electrolytic capacitors in order to regulate and stabilize the dc-bus voltage. In some cases, multilevel converters are used to form the power electronics interface in the drivetrain. The topology of the multilevel converters can be an H-bridge back-to-back converter or a neutral-point-clamped back-to-back converter [17, 22]. Most wind turbine topologies either have a dc-bus formed by electrolytic capacitors or a dc-link formed by inductors. The electrolytic capacitors are one of the most failure-prone components that adversely impact the system reliability [5]. The failure of these capacitors has a significant impact on the maintenance cost especially in the case of offshore wind turbines [13, 23]. The dc-link inductor is bulky and adds to the system loss reducing the system's efficiency [19]. In some cases, the grid side converter is located away from the wind turbine and the transmission cable is used to realize the dc-link inductor [20]. Additionally, the lack of gearbox in the DDWT increases the size of the PMSG and the capital cost of the overall system [13, 23–25]. In the following, the proposed DDWT topology is described.

2.3 Proposed DDWT topology

The proposed topology for the DDWT is presented in **Figure 2**. In this subsection, different parts of the proposed topology are explained. First, the power electronics interface topology is presented, and then, the PMSG design flexibility provided by implementing the boost CSI is described.

2.3.1 The power electronics interface

The power electronics interface in the proposed topology is a back-to-back converter made up of a three-phase VSC and a boost CSI, as shown in **Figure 2**. The boost CSI is equipped by Reverse Blocking IGBTs (RB-IGBT), and no dc-bus capacitor or dc-link inductor exists in the proposed DDWT. As a result of avoiding the dc-bus capacitor, the system mean-time-between-failure can significantly be improved in comparison with the conventional VSC-based systems [26]. While any CSI requires an inductor at the dc-link, the proposed DDWT eliminates the dc-link inductor by utilizing the generator synchronous inductance, L_s [15]. In order to achieve a Total Harmonic Distortion (THD) of the current waveforms at the inverter output acceptable under the IEEE 1547–2018 interconnection standards, the operation of the boost CSI must always be in Continuous Conduction Mode (CCM). The minimum dc-link inductance, L_{dc} required to keep the inverter in CCM has been derived in [27]. However, the synchronous inductance, L_s, will be less than the L_{dc}, i.e. $L_s = \sqrt{3/2}\, L_{dc}$. This is because Thevenin's equivalent inductance of the generator-converter from the dc-bus is almost $(3/2)\, L_s$ and $I_{rms} \approx \sqrt{2/3}\, I_{dc}$. Also, a traditional CSI operated using space vector PWM switching provides a maximum

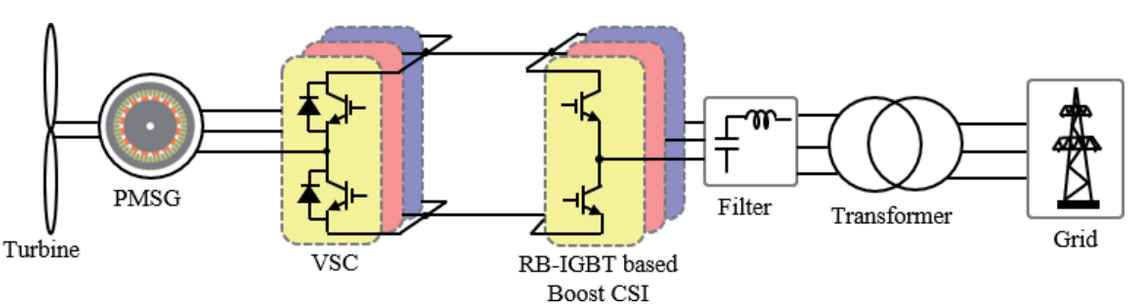

Figure 2.
The proposed wind turbine system topology with PMSG connected to a VSC and the boost inverter equipped by RB-IGBTs.

boost ratio, V_{LLrms}/V_{dc}, of about 1.2 [28]. However, the boost CSI is modulated using the Phasor Pulse Width Modulation (PPWM) switching technique, providing a boost ratio more than three [29–31]. As a result, a low voltage PMSG design will be possible for the proposed DDWT. The advantages gained by using a low voltage generator are discussed in the next subsection.

2.3.2 The permanent magnet generator

The low dc-side voltage required by the boost CSI enables a low output ac-voltage from the PMSG. In a traditional DDWT topology, the voltage at the generator and the grid should have almost the same rms value [32, 33]. However, if the developed topology is utilized, then, for example, $120V_{LLrms}$ from the PM generator is sufficient to generate an rms line-to-line voltage of 480 V at the converter output. As described in [15], consider the emf equation $E \propto N_{ph} p\, \omega_m \phi_p$, where, E is the peak induced voltage per phase, N_{ph} is the number of winding turns per phase, ω_m is the mechanical angular velocity, p is the total number of poles, and ϕ_p is the maximum magnetic flux per pole, [33]. Here ω_m is dependent on the wind speed, and the fundamental magnetic flux per pole is obtained from $\phi_p \cong (4/\pi) B_m (2\pi/p)(D/2)l = 4Dl B_m/p$, where D is the mid-airgap diameter, B_m is the flux density, and l is the stack length. Accordingly, for a given angular velocity, permanent magnet material, and air-gap height, l_g one can say $E \propto N_{ph} Dl$, which means that a generator with a lower output voltage requires a lower value of $N_{ph} Dl$. On the other hand, the minimum synchronous inductance, required for the boost CSI to operate in CCM, restricts the maximum number of poles, since $L_s \propto (Dl/l_g)(N_{ph}/p)^2$ [33]. Hence, the desired values of the generator output voltage, $(E^2 - (\omega_s L_s I)^2)^{1/2} \cong E$ and synchronous inductance, L_s, are herein used as the PMSG design inputs for a given rated power.

3. Generator design and comparison

In this section, a 1.5 MW PMSG is designed for the proposed DDWT topology and then the design is compared with an existing 1.5 MW PMSG [34].

3.1 New generator design

The generator is designed using GenAC toolbox of MagneForce Finite Element (FE) software. The designed machine is a low-speed, concentrated overlapping tooth coil double layered winding, three-phase PMSG rated at 1.5 MW. The generator is designed to be radial flux, cylindrical rotor, rotor surface mounted pole machine so that it can be compared with the existing 1.5 MW PMSG [34]. For the sake of comparison, both the existing and new 1.5 MW systems have the rated speed of 19.65 rpm, and the same generator airgap of 0.6 mm. Also, the line-to-line voltage of the new generator is 450 V, while the existing generator line-to-line voltage is 770 V, see **Table 1**.

Figure 3 shows the cross-sectional view of the new generator, including the stator slot and tooth dimensions in details. Moreover, the insulation thickness in each slot is 3.5 mm. The overall slot-fill is about 62%. Also, the rotor shaft bore diameter is 700 mm. The stator bore diameter is 3500 mm, the stator length is 600 mm, and the airgap length, l_g, is 0.6 mm. The PM material is sintered Neodymium Iron Boron (NdFeB) with the maximum residual flux density of B_r = 1.2 T, and maximum coercive force of 24 k Oersted (i.e. H_c =1910 kA/m). The permanent magnet pole dimension is as 260 × 100 mm^2 with a pole arc to pole pitch ratio of 0.8. **Figure 4** demonstrates the electromagnetic flux and the flux density distribution over the

Parameter	Existing generator	Designed (new) generator
Power rating	1.5 MW	1.5 MW
Speed	19.65 rpm	19.65 rpm
Air gap length	0.6 mm	0.6 mm
Line-to-line voltage	770 V	450 V

Table 1.
The existing and new generator input parameters.

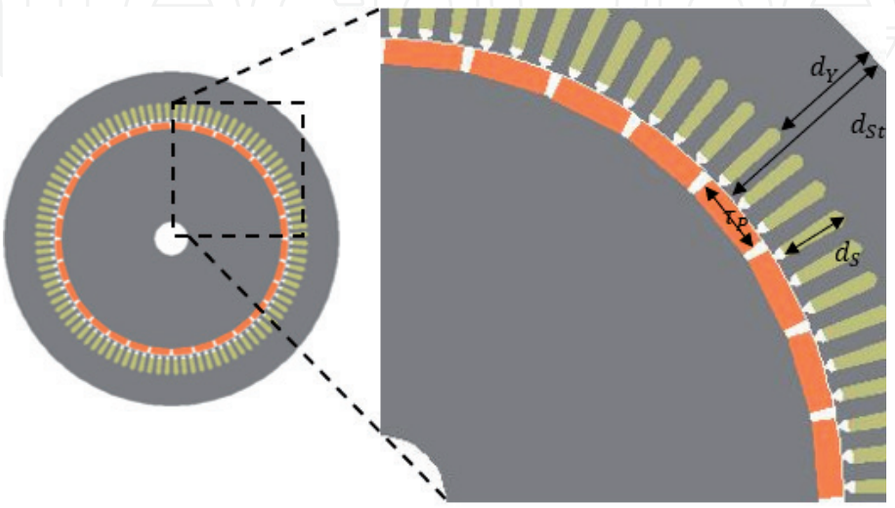

Figure 3.
Cross sectional view of the new design 1.5 MW PMSG.

PMSG at 1 $p.u.$ load. As can be seen in **Figure 4**, the generator is not saturated at rated load. The maximum flux density is observed at the stator tooth, and the maximum airgap flux density measured using FE computations is about 1.15 T. Using circuit simulation for the new design, ~20 mH is needed to keep the dc-link current in CCM for different load levels.

3.2 Generator parameter comparison

In this subsection, the designed PMSG is compared with an existing 1.5 MW PM generator for DDWT [34]. **Table 2** shows the differences between the new and existing design parameters. In order to compare the two generators, the existing generator design is duplicated using the FE software. The design parameters for the existing generator are obtained from [34]. The comparison of the generator no-load line-to-line voltage, and the flux linkage with respect to rotor electrical position is presented in **Figure 5**. The no-load line-to-line voltage waveforms are shown in **Figure 5(a)**. The flux linkage of phase-A of the generator versus the rotor electrical position is presented in **Figure 5(b)**. As can be seen in **Figure 5(b)** that there is minimal distortion in the flux linkage, and it is sinusoidal for the generator designed. Furthermore, **Figure 5(b)** shows that the flux linkage is higher for the new design than the existing generator, as the new design has higher per phase inductance than that of the existing generator. It should be noted that even though the flux is higher in the new generator design, the maximum flux density is less than that permissible for the core, i.e. 1.2 T. As shown in **Table 2**, the number of

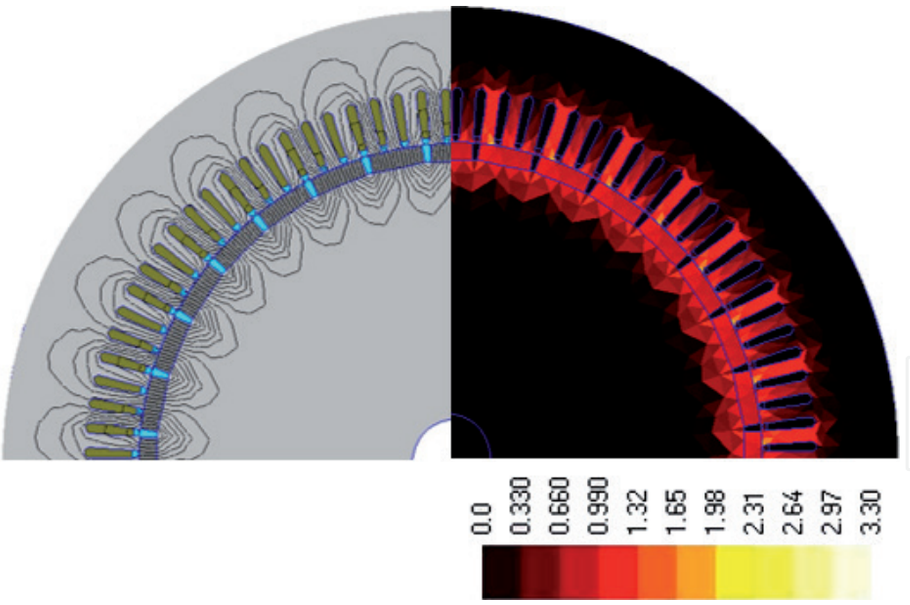

Figure 4.
Flux and flux density distribution (T) over the cross-section of the designed PMSG at full load.

Parameter	Existing generator	Designed (new) generator
No. of poles, p	78	32
Airgap flux density, B_{max}	1.01 T	1.15 T
Winding current density, J	4 A/mm^2	6 A/mm^2
Linear current density	31.08 kA/m	36.60 kA/m
Stator winding factor, k_w	0.942	0.951
Stator q-axis inductance, L_q	12.20 mH	20.16 mH
Stator d-axis inductance, L_d	12.19 mH	20.11 mH
Stator inner diameter	4462 mm	3500 mm
Stack length	500 mm	600 mm
Number of slots	234	96
Winding turns per phase	56	30
Copper weight	384.4 kg	401.3 kg
Core weight (stator)	21,552 kg	19,429 kg
Rotor weight	40,990 kg	35,870 kg

Table 2.
Comparison of the designed vs. existing generator.

poles in the existing generator is 78 which has been reduced to less than half in the new design to 32 poles. Also, each pole volume is 600 × 260 × 100 mm^3 in the new design, whereas, in the existing PMSG, each pole volume is 500 × 142 × 100 mm^3. Thus, the total permanent magnet material is reduced by 9.8% in the new design. The reduction in the permanent magnet material reduces the dependency on the imported and highly unstable market of NdFeB materials.

The FE measured linear current density for the new design is 36.6 kA/m at the pole surface, as shown in **Table 2**, while the NdFeB coercive force is 1910 kA/m. In **Table 3**, the demagnetization of PM poles is computed for different output power factors and the results are presented. The computation of demagnetization is done using the MagneForce FE software. The software calculates the total flux with

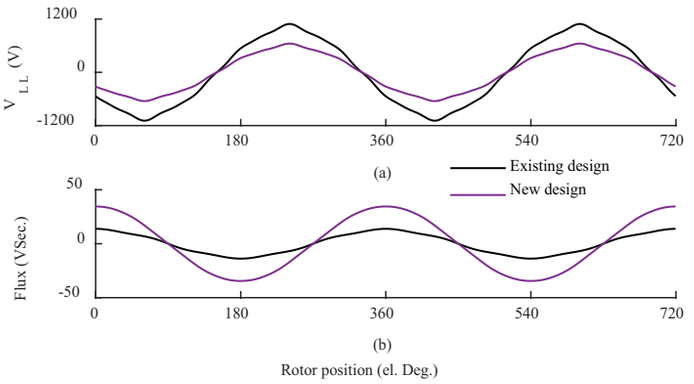

Figure 5.
Generator (a) line-to-line voltage, and (b) phase flux linkage vs. rotor electrical position obtained through FE computations for the existing and new design of the generators.

	pf **= 0.95**	**0.85**	**0.75**
		Demagnetization (%)	
Existing design	0.080	0.075	0.078
New design	0.084	0.080	0.081

Table 3.
Percent demagnetization of pm poles for varying output power factor and s = 1 p.u. using FE computations.

virgin (non-demagnetized) magnets. It then runs the simulation and keeps track of the worst demagnetization that each element within the rotor pole experiences throughout a complete ac cycle. The FE software uses the demagnetized elements to re-construct the magnet, and then, calculates the total flux from this demagnetized magnet. Finally, the software calculates the percentage drop in total flux from the virgin magnets to the demagnetized magnets and reports the difference as the amount of demagnetization. It should be noted that the demagnetization analysis is based on loading of the generators and total flux drop, and it does not take into account the thermal models for the generators.

A normalized comparison of the copper and core losses, rotor and stator weights, and the volume of the two generators is presented in **Figure 6**. In **Table 4**, the efficiency, as well as core and copper losses, are provided for different power factors and a constant apparent power, i.e. S =1 p.u. The base values for the per-unit (p.u.) calculations are S_{base} =1.5 MVA, and V_{base} =690 V. As can be observed, the copper loss in the new generator increases. This is due to the higher current level in the low-voltage generator. Although the new design has lower number of turns in the generator winding – lower overall stator resistance – the line current is higher, which results in higher copper loss in the new low voltage generator. Nevertheless, the core loss for the designed low voltage generator decreases by about 9.5%. This reduction in the core loss in the new designed generator is due to the reduction in the number of poles in the new designed generator, which results in a substantial decrease in the generator output voltage and frequency, see **Table 2**. It can be observed that the generator efficiency is not compromised with full load efficiency of the new and existing generator being 94.4 and 93.8%, respectively, while the stator and rotor dimensions are significantly decreased. The no-load core-losses for the existing and new generator designs are computed to be 0.040 p.u. and 0.0351 p.u., respectively. The change in core losses from no-load to full load can be attributed to the armature reaction, see **Table 4**. It should be noted that the losses and efficiency data presented in in **Table 4**, and **Figure 6** are

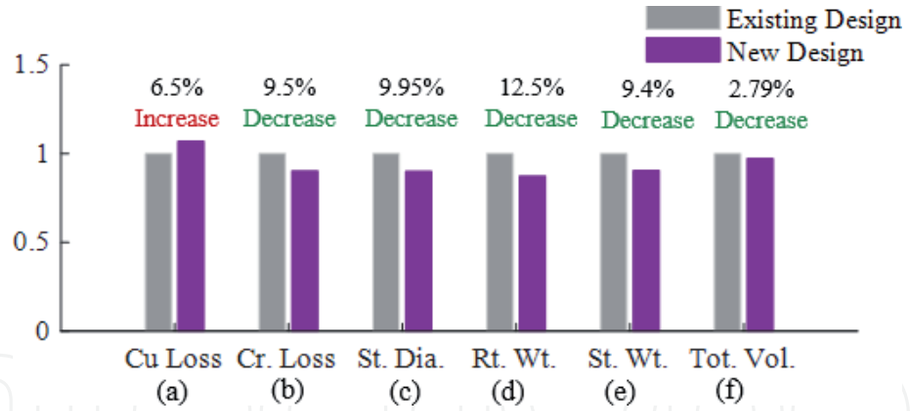

Figure 6.
Comparison of normalized (a) copper loss, (b) core loss, (c) stator diameter, (d) rotor weight, (e) stator weight, and (f) volume of the existing and designed PM generator for DDWT using FE computation.

	pf =	**0.95**	**0.85**	**0.75**
Copper Loss (*pu*.)	Existing	0.0245	0.0245	0.0250
	New	0.0268	0.0269	0.0278
Core Loss (*pu*.)	Existing	0.0405	0.0405	0.0405
	New	0.0353	0.0354	0.0354
Efficiency (%)	Existing	93.50	93.49	93.45
	New	93.79	93.77	93.68

Table 4.
Core loss, copper loss, and efficiency for varying output power factor and S = 1 p.u. using FE computations.

obtained using the FE models of the PMSGs. A comparison of the rotor and stator weights, respectively, for the two generators is presented in **Figure 6**. The rotor weight is the cumulative weight of the NdFeB PM poles and the rotor core. Similarly, the stator weight presented in the combined weight of the armature windings and the stator core. The stator and rotor weight reductions for the new generator are ~9.4 and 12.5%, respectively. Additionally, the overall volume of the new generator is reduced by ~ 2.79% than the existing design. It can be observed that the decrease in the stator diameter (which is about 10%) does not render to a comparable reduction in the overall volume of the new generator. This is due to the higher stack length of the new generator. The designed generator has a stack length to diameter (l/D) ratio of 0.13 as compared to the existing generator design with l/D ratio of 0.11. The decrease in the generator volume and weight along with the elimination the failure prone dc-bus capacitor and circumventing the dc-link inductor needed in CSIs will further render into decreased capital cost of the overall system. The simulation and experimental results evaluating and validating the performance of the proposed topology of the DDWT are presented in the following sections.

4. System controls

In this section, first, the control technique implemented for the developed topology is briefly explained. The developed system is controlled with generator side VSC being modulated for power transfer to the grid and the boost inverter modulated to stabilize the input dc-voltage.

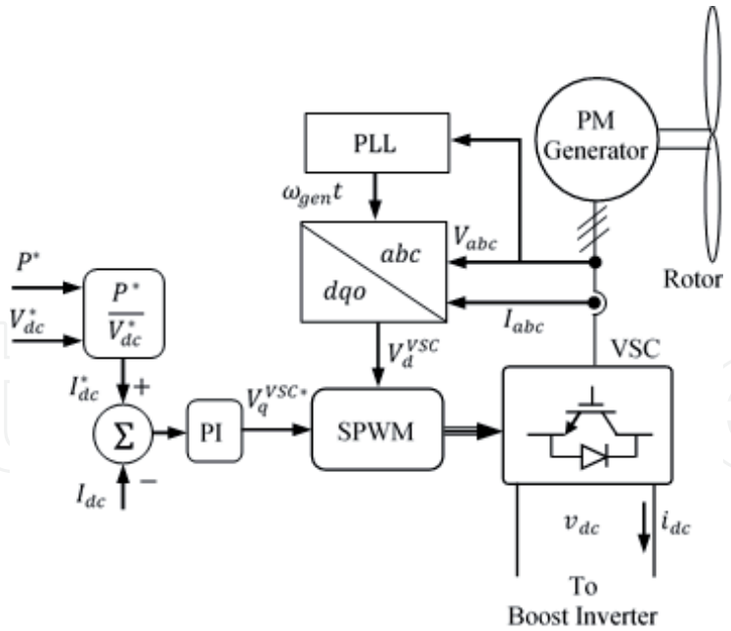

Figure 7.
Block diagram of controller for the VSC [26].

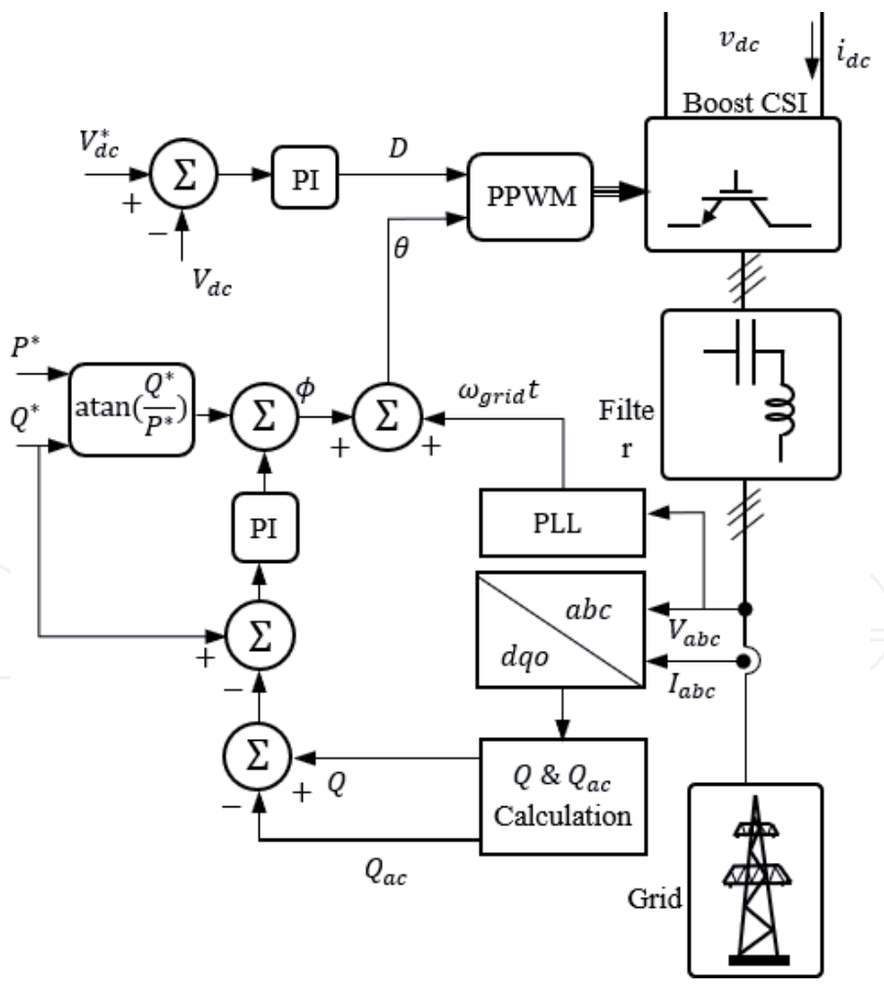

Figure 8.
Block diagram of controller for the single-stage boost inverter [26].

The power electronics interface proposed for the DDWT drivetrain is controlled to regulate the power injected to the grid and to maintain the average dc-side voltage. The generator side VSC is modulated to inject desired power to the dc-side.

Figure 7 shows the block diagram of the controller for VSC. The generator line-to-line voltages and dc-side voltage and current are the measured feedback received by this controller. The ac side signals are then converted to the *dqo* reference frame. The desired active power on the grid side, P^* is compared to the measured power on the dc side. The error is then mitigated by using a Proportional-Integral (PI) controller which then generates the desired *q*-axis converter voltage, V_q^{VSC*}. The generated *q*- axis voltage and the measured *d*-axis voltages serve as base to generate the switching signal for the VSC. The controller is equipped with one of the existing MPPT techniques, e.g. $P^* = K_{opt}\omega_R^3$, [36, 37].

Figure 8 shows the block diagram of the controller for the boost CSI. The controls for this converter help regulate the dc-side voltage and to modulate the reactive power injected into the grid. Thus, the controller for the VSC helps modulate the active power injected into the grid and the controller for the boost CSI modulates the reactive power into the grid. The inputs to the boost CSI controller are the measured grid-side line-to-line voltages, line currents and dc-side. The three-phase signals are converted to the *dqo* reference frame. The *dqo* quantities are used to compute the reactive power injected to the grid, which is compared to the reference reactive power. The error is then mitigated using a PI controller which generates the reference angle, θ for the boost inverter. Similarly, the dc-side voltage, V_{dc} (where, $V_{dc} = \langle v_{dc} \rangle$) is compared to the desired dc-side voltage, V_{dc}^* and a PI controller is used to generate the modulation index, *D* for the implementing the PPWM switching technique [26]. The details on the PPWM technique has been provided in [29–31].

5. Simulation results

This section presents the simulation results for the evaluation of the feasibility and performance of the developed topology of the DDWT. The software platform used for these evaluations is MATLAB/Simulink environment using SimPowerSystems toolbox. The simulated system uses the FE design of the generator as presented in Section 3. The switching frequency of 6 kHz is used for both the VSC and the boost CSI. The switching methodology for the VSC is the Sine PWM (SPWM) technique while the boost CSI employs the PPWM switching technique [29, 30]. As described in the previous section, the VSC controller modulates the active power transfer injected into the grid and the boost CSI controller regulates the dc-side voltage and controls the reactive power injected into the grid. A detailed discussion on these controllers and their performance is presented in [26]. The output filter parameters for the boost CSI are C_f = 20 μF and L_f = 5 mH.

The quality of the output waveforms of the proposed system is demonstrated in **Figures 9** and **10**. **Figure 10** presents the steady-state waveforms of generator line-to-line voltage and line current when the generator speed is 18.75 rpm. The power converters were modulated to inject 1 MW (0.67 p.u.) P into the grid at unity power factor (UPF). The boost CSI controller was regulating the dc-side voltage at 500 V. **Figure 10(a)** and **(b)** show that the THD of the generator output line current is ~1.2%, which further ensures less harmonics transferred to the generator side and eliminates the low-frequency torque ripple on the generator shaft. **Figure 9** presents the waveforms of the boost CSI output line-to-line voltage at the point of common coupling, and line current injected into the grid. The grid line current THD is computed to be ~3.3%, which is complaint of the IEEE 1547–2018 interconnection standards [38].

Figure 11 presents the dynamic behavior of the proposed DDWT system. The generator speed, three-phase line-to-line voltage waveforms at the point of common coupling (PCC), three-phase generator line current waveforms, and the dc-side current are shown in **Figure 11**. The first event occurs at t = 1*s*, when the generator speed

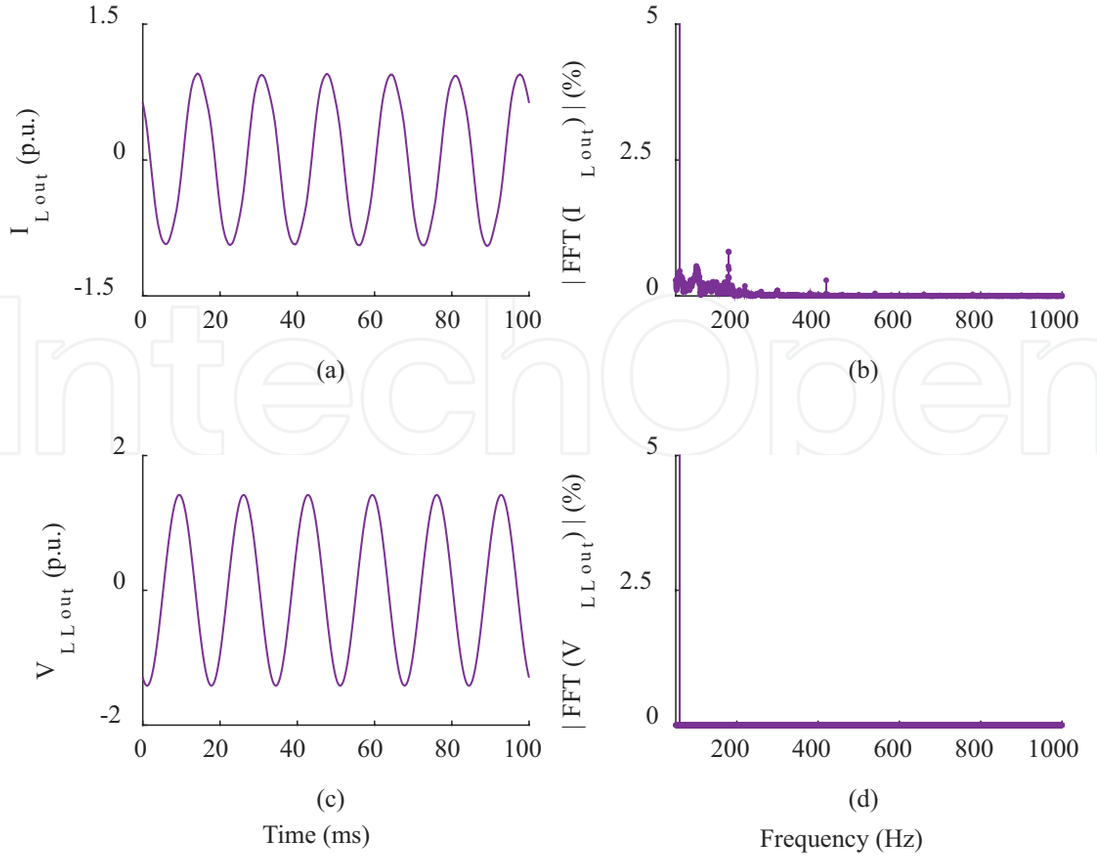

Figure 9.
Simulated results of inverter output (a) line current waveform, (b) line current FFT analysis, (c) line-to-line voltage waveform, and (d) line-to-line voltage FFT analysis for grid-tied system the generator speed is 18.75 rpm and the system is injecting 0.67p.u. Active power into the grid [35].

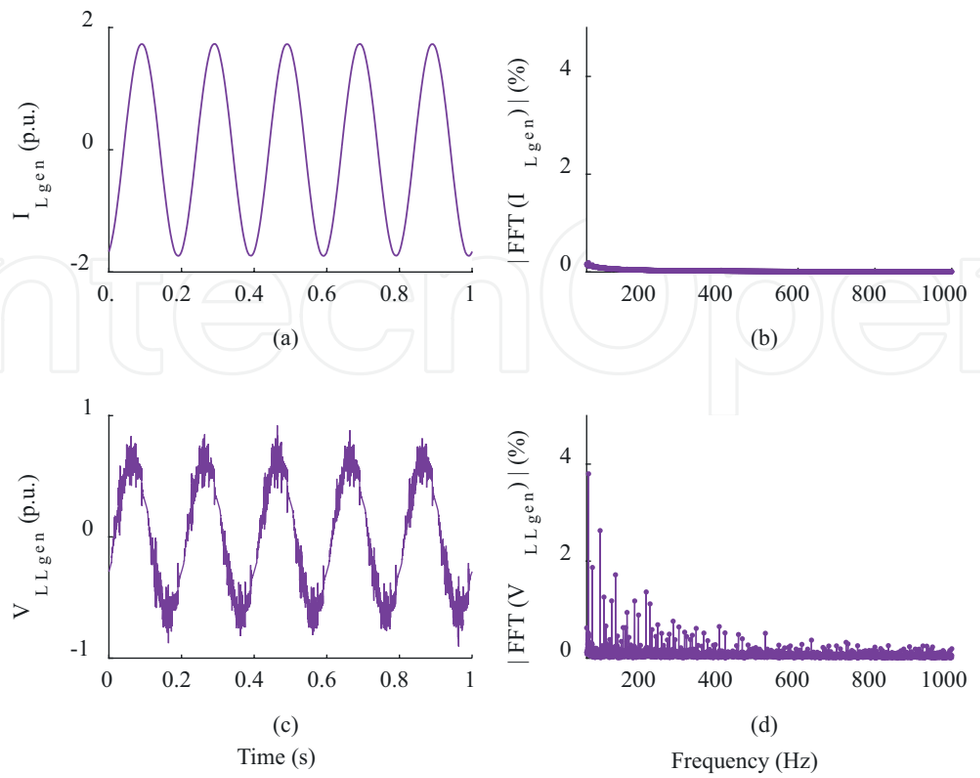

Figure 10.
Simulated results of generator output (a) line current waveform, (b) line current FFT analysis, (c) line-to-line voltage waveform, and (c) line-to-line voltage FFT analysis, for grid-tied system when the generator speed is 18.75 rpm and it is supplying [35].

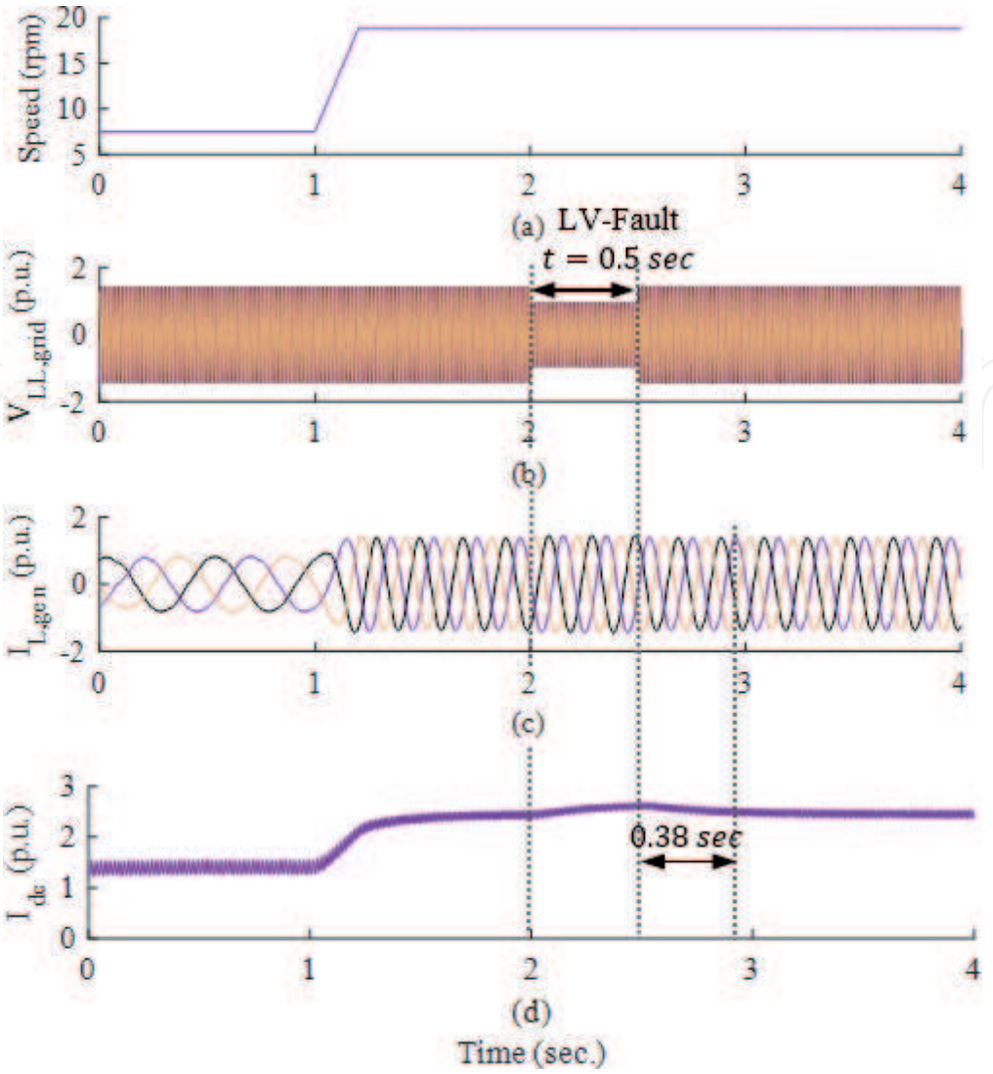

Figure 11.
Plot of (a) PMSG speed, (b) three-phase line-to-line voltage at the PCC, (c) three-phase generator line current, and (d) dc-side current showing system behavior for varying wind speed and three-phase low-voltage fault at the grid [35].

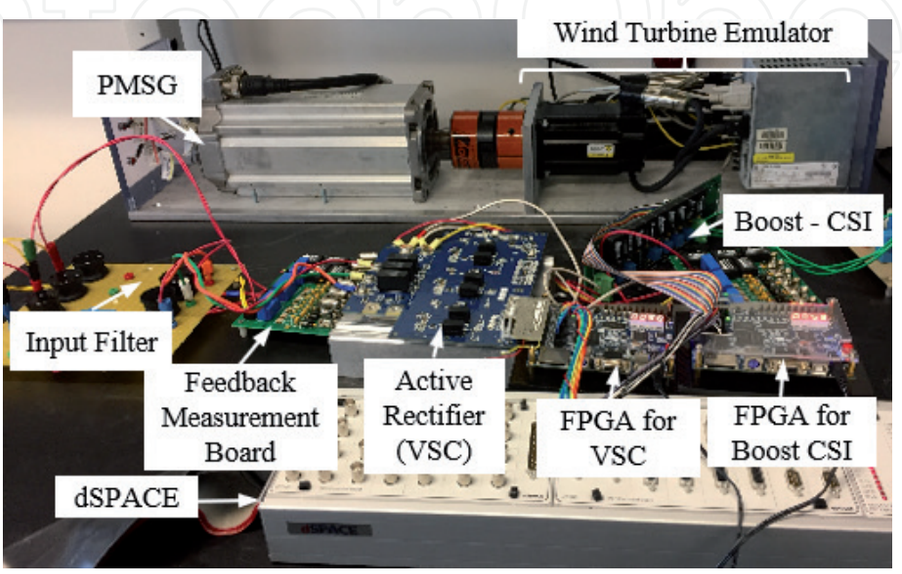

Figure 12.
Laboratory scale 1.5 kW, setup for the proposed DDWT topology [35].

changes gradually from 7.5 rpm to 19.65 rpm. The sudden speed changes shown in **Figure 11** are not realistic and is just used as a case to evaluate the robustness of the system controls. **Figure 11(c)** and **(d)** show that the system easily tracks the maximum available wind power. The fault ride-through capability of the system is also evaluated. This is done by simulating a three-phase low-voltage fault on the inverter terminals at $t = 2\,s$, where the grid voltage decreases by 35% and the fault is cleared after 0.5s [39]. The developed system rides-through this low-voltage seamlessly and starts normal operation again in ~0.38s after the clearing of the fault.

6. Experimental evaluation results

The feasibility of the developed DDWT topology is evaluated using experimental results from 1.5 kW, 240V_{LL} laboratory scale prototype, in this section (see **Figure 12**). In this setup, a motor-drive system is used as the wind turbine emulator that runs a commercially available PMSG, which feeds a three-phase 50Ω resistive load through the proposed back-to-back converter and a CL filter. The filter values are $C_f = 20\ \mu$F and $L_f = 5$ mH, when $f_s = 6$ kHz for the boost CSI. For the first test case to evaluate if the generator synchronous inductance can be utilized in place of the dc-link inductor, a diode bridge rectifier is used as the generator side. The waveforms of the generator line current, generator line-to-line voltage, load line current, and load line-to-line voltage are shown in **Figure 13**. The PMSG produces rms line-to-line voltage of 45 V at 30 Hz. This is boosted to an output load line-to-line voltage of 208 V at 60 Hz by the boost CSI. The generator current and load current

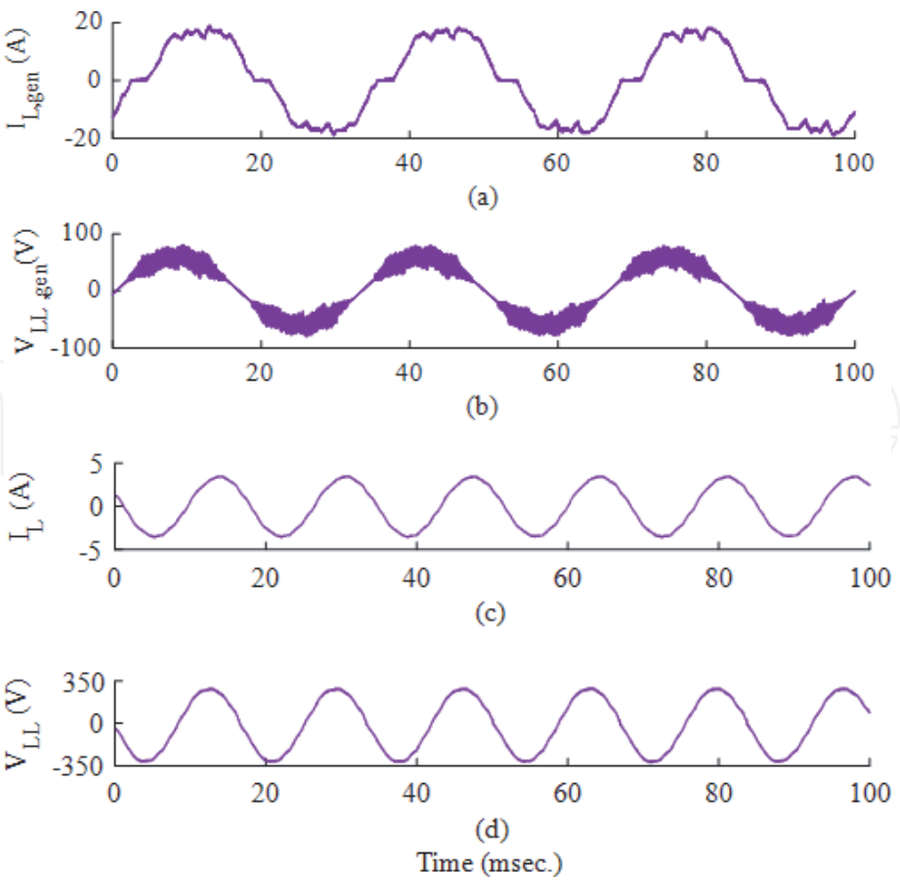

Figure 13.
Experimentally obtained waveforms of the (a) generator line current, (b) generator line-to-line voltage, (c) load line current, and (d) load line-to-line voltage when the generator is rotating at 450 rpm (30 Hz), the output is regulated at 208 V, and the generator side converter is a diode bridge rectifier [35].

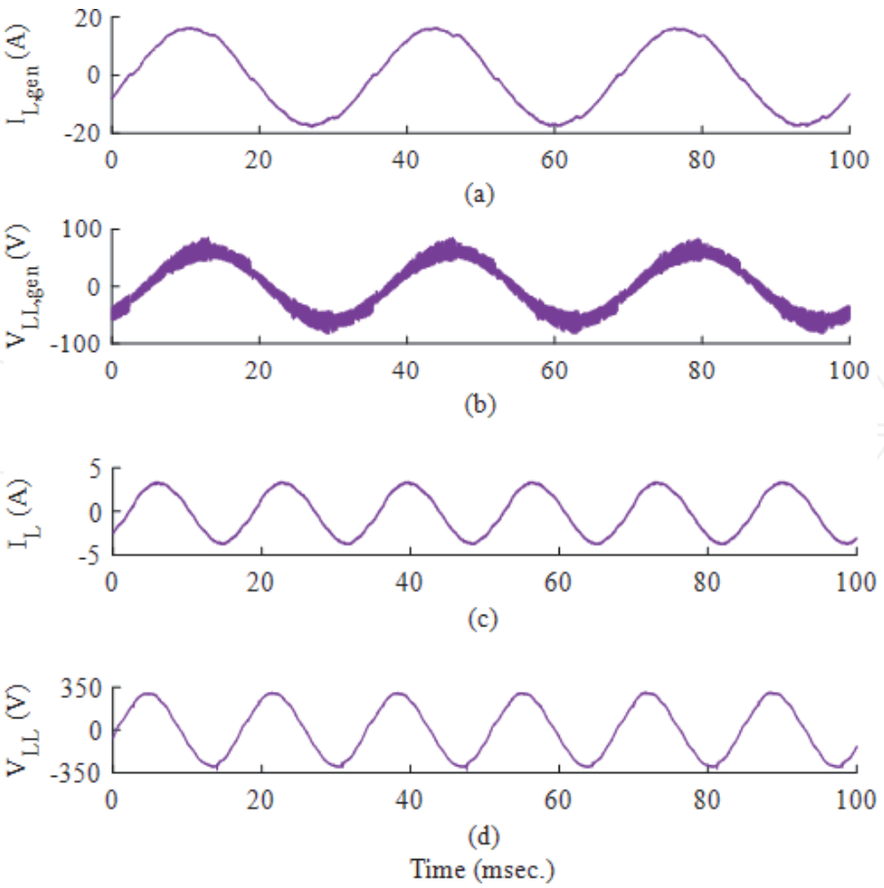

Figure 14.
Experimentally obtained waveforms of the (a) generator line current, (b) generator line-to-line voltage, (c) load line current, and (d) load line-to-line voltage when the generator is rotating at 450 rpm (30 Hz) and the output is regulated at 208 V with the generator side converter as VSC [35].

THDs are measured to be 33.1 and 3.0%, respectively. For the next test case, the generator side converter employed is a VSC. **Figure 14** shows the waveforms of the same quantities for this test case. The switching frequency for the VSC is f_s = 25 kHz. The average dc side voltage was maintained at 70 V. The generator current and load current THDs are measured to be 2.9 and 2.8%, respectively The evaluation results presented in **Figures 13** and **14** demonstrate the capability of the developed systems to utilize the generator synchronous inductance, while still maintain the quality of the system output.

7. Conclusion

In this chapter, an inductorless generator-converter topology has been presented for DDWTs. This paper also presents a new topology of power electronics interface for the DDWTs. The grid side VSC used in a conventional DDWT has been replaced by a boost CSI. The dc-link inductor inherently required in a CSI topology has been eliminated by using the synchronous inductance of the PMSG. This topology has further facilitated the elimination of vulnerable dc-bus electrolytic capacitors, thereby increasing the overall system reliability. Furthermore, less frequent failures of the capacitors will lead to increase in system availability, resulting in substantial decrease in the maintenance costs. In this chapter, FE analysis is used to design and evaluated a 1.5 MW generator for the proposed system. The FE analysis is also used to compare the designed and an actual generator. The advantages of using the proposed topology have been demonstrated through reduction in generator weight,

volume, and amount of PM material. The controls for the proposed system have also been discussed in this chapter. The feasibility and performance of the proposed DDWT system has been validated through simulation results and experimental results from a laboratory scale prototype, in this chapter.

Author details

Akanksha Singh
National Renewable Energy Laboratory, Golden, USA

*Address all correspondence to: akanksha.singh@nrel.gov

References

[1] Global Wind Energy Council Report. [Online] Available from: http://www.gwec.net/global-figures/wind-in-numbers/

[2] AWEA U.S. Wind Industry Market Reports for 2015 [Online]. Available from: http://www.awea.org

[3] Manwell J, Mcgowan J, Rogers A. Wind Energy Explained: Theory, Design, and Applications. Second ed. United Kingdom: Wiley; 2011

[4] Ribrant J, Bertling L. Survey of failures in wind power systems with focus on swedish wind power plants during 1997-2005. IEEE Transactions on Energy Conversion. 2007;**22**(1):167-173

[5] Daneshi-Far Z, Capolino GA, Henao H. Review of failures and condition monitoring in wind turbine generators. In: International Conference on Electrical Machines. 2010

[6] Tavner P, Bussel G, Spinato F. Machine and converter reliabilities in wind turbines. In: IEEE International Conference on Power Electronics, Machines and Drives. Dublin, Ireland; 2006

[7] Polinder H, Van Der Pijl FFA, de Vilder GJ, Tavner P. Comparison of direct-drive and geared generator concepts for wind turbines. IEEE Transactions on Energy Conversion. 2006;**21**(3):725-733

[8] Spinato F, Tavner PJ, van Bussel GJW, Koutoulakos E. Reliability of wind turbine subassemblies. IET Renewable Power Generation. 2009;**3**(4):387-401

[9] Liserre M, Cardenas R, Molinas M, Rodriguez J. Overview of multi-MW wind turbines and wind parks. IEEE Transactions on Industrial Electronics. 2011;**58**(4):1081-1095

[10] Wang H, Liserre M, Blaabjerg F. Toward reliable power electronics: Challenges, design tools, and opportunities. IEEE Industrial Electronics Magazine. 2013;**7**(2):17-26

[11] Chen J, Chen W, Li J, Zhang X, Sun P. Lifetime assessment of DC link electrolytic capacitor of wind power converter based on operational condition. In: 2016 IEEE International Conference on High Voltage Engineering and Application (ICHVE), Chengdu. 2016. pp. 1-4

[12] Leban K, Ritchie E, Argeseanu A. Design preliminaries for direct drive under water wind turbine generator. In: IEEE International Conference on Electrical Machines. Marseille, France; 2012

[13] Mcmillan D, Ault GW. Techno-economic comparison of operational aspects for direct drive and gearbox-driven wind turbines. IEEE Transactions on Energy Conversion. 2010;**25**(1):191-198

[14] Chen Z, Guerrero JM, Blaabjerg F. A review of the state of the art of power electronics for wind turbines. IEEE Transactions on Power Electronics. 2009;**24**(8):1859-1875

[15] Singh A, Mirafzal B. Indirect boost matrix converter and low-voltage generator for direct drive wind turbines. The Journal of Engineering. 2018;**2018**(1, 1):10-16

[16] Singh A, Mirafzal B. A generator-converter design for direct drive wind turbines. In: Proc. IEEE ECCE. 2016

[17] Blaabjerg F, Liserre M, Ma K. Power electronics for wind turbine systems. IEEE Transactions on Industry Applications. 2012;**48**(2):708-719

[18] Lumbreras C, Guerrero JM, Garcia P, Briz F, Reigosa DD. Control of a small wind turbine in the high wind speed

region. IEEE Transactions on Power Electronics. 2016;**30**(10):6980-6991

[19] Dai J, Xu DD, Wu B. A novel control scheme for current-source converter-based PMSG wind energy conversion systems. IEEE Transactions on Power Electronics. 2009;**24**(4):963-972

[20] Tenca P, Rockhill AA, Lipo TA, Tricoli P. Current source topology for wind turbines with decreased mains current harmonics, further reducible via functional minimization. IEEE Transactions on Power Electronics. 2008;**23**(3):1143-1155

[21] Lee JS, Lee KB, Blaabjerg F. Open-switch fault detection method of a back-to-back converter using NPC topology for wind turbine systems. IEEE Transactions on Industry Applications. 2015;**51**(1):325-335

[22] Blaabjerg F, Ma K. Future on power electronics for wind turbine systems. IEEE Journal of Emerging and Selected Topics in Power Electron. 2013;**1**(3):139-151

[23] Zavvos A, Mcdonald A, Mueller M. Optimisation tools for large permanent magnet generators for direct drive wind turbines. IET Renewable Power Generation. 2013;**7**(2):163-171

[24] Zhang Z, Zhao Y, Qiao W, Qu L. A space-vector-modulated sensorless direct-torque control for direct-drive PMSG wind turbines. IEEE Transactions on Industry Applications. 2014;**50**(4):2331-2441

[25] Potgieter JHJ, Kamper MJ. Design optimization of directly grid-connected PM machines for wind energy applications. IEEE Transactions on Industry Applications. 2015;**51**(4):2949-2958

[26] Singh A, Mirafzal B. Three-phase single-stage boost inverter for direct drive wind turbines. In: 2016 IEEE Energy Conversion Congress and Exposition (ECCE). Milwaukee, WI; 2016. pp. 1-7

[27] Singh A, Mirafzal B. A low-voltage generator-converter topology for direct drive wind turbines. In: 2016 IEEE 7th International Symposium on Power Electron. For Distributed Gener. Sys. (PEDG). Vancouver, BC; 2016. pp. 1-6

[28] Wang Z, Wu B, Xu D, Zargari NR. A current-source-converter-based high-power high-speed PMSM drive with 420-Hz switching frequency. IEEE Transactions on Industrial Electronics. 2012;**59**(7):2970-2981

[29] Mirafzal B, Saghaleini M, Kaviani A. An SVPWM-based switching pattern for stand-alone and grid-connected three-phase single-stage boost inverters. IEEE Transactions on Power Electronics. 2011;**26**(4):1102-1111

[30] Singh A, Milani AA, Mirafzal B. Modified phasor pulse width modulation method for three-phase single-stage boost inverter. In: 2014 IEEE Applied Power Electron. Conf. And Expo. - APEC 2014. Fort Worth, TX; 2014. pp. 1276-1280

[31] Singh A, Kaviani AK, Mirafzal B. On dynamics models and stability of three-phase phasor PWM based CSI for stand-alone applications. IEEE Transactions on Industrial Electronics. May 2015;**62**(5):2698-2707

[32] Holmes DG, Lipo TA. Pulse Width Modulation for Power Converters: Principles and Practice. First ed. New York, USA: John Wiley & Sons; 2003

[33] Fitzgerald AE, Kingsley C Jr, Umans SD. Electric Machinery. Sixth ed. New York, USA: McGraw Hill; 2003

[34] Northern Power NW 1500 Direct-Drive Generator –Report, [Online] Available from: http://www.nrel.gov/docs/fy08osti/40177.pdf

[35] Singh A, Benzaquen J, Mirafzal B. Current source generator–converter topology for direct-drive wind turbines. IEEE Transactions on Industry Applications. March-April 2018;**54**(2):1663-1670

[36] Fateh F, White WN, Gruenbacher D. A maximum power tracking technique for grid-connected DFIG-based wind turbines. IEEE Journal of Emerging and Selected Topics in Power Electronics. 2015;**3**(4):957-966

[37] Yuan X, Li Y. Control of variable pitch and variable speed direct-drive wind turbines in weak grid systems with active power balance. IET Renewable Power Generation. 2014;**8**(2):119-131

[38] IEEE standard for interconnection and interoperability of distributed energy resources with associated electric power systems interfaces. In: IEEE Std 1547-2018 (Revision of IEEE Std 1547-2003). 2018. pp. 1-138

[39] Xiang D, Turu JC, Muratel SM, Wang T. On-site LVRT testing method for full-power converter wind turbines. IEEE Transactions on Sustainable Energy. 2017;**8**(1):395-403